A Universal Method to Produce Low–Work Function Electrodes for Organic Electronics

Yinhua Zhou *et al.*

Science **336**, 327 (2012);
DOI: 10.1126/science.1218829

Science (print ISSN 0036-8075; online ISSN 1095-9203) is published weekly, except the last week in December, by the American Association for the Advancement of Science, 1200 New York Avenue NW, Washington, DC 20005.

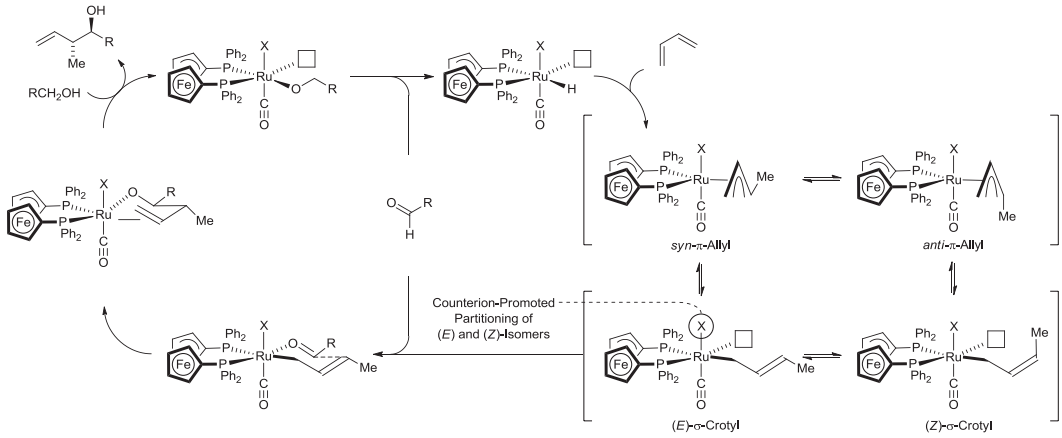

Fig. 3. Proposed mechanism for ruthenium-catalyzed hydrohydroxyalkylation of butadiene, illustrating the counterion-dependent partitioning of (*E*)- and (*Z*)-σ-crotylruthenium isomers.

References and Notes

1. M. Butters *et al*., *Chem. Rev.* **106**, 3002 (2006).
2. R. A. Sheldon, E. The, *Green Chem.* **9**, 1273 (2007).
3. C. A. Busacca, D. R. Fandrick, J. J. Song, C. H. Senanayake, *Adv. Synth. Catal.* **353**, 1825 (2011).
4. J. Magano, J. R. Dunetz, *Chem. Rev.* **111**, 2177 (2011).
5. C. D. Frohning, C. W. Kohlpaintner, in *Applied Homogeneous Catalysis with Organometallic Compounds*, B. Cornils, W. A. Herrmann, Eds. (Wiley-VCH, Weinheim, Germany 1996), pp. 29–104.
6. P. W. N. M. van Leeuwen, in *Homogeneous Catalysis: Understanding the Art* (Kluwer, Dordrecht, Netherlands, 2004), pp. 139–174.
7. J. F. Bower, M. J. Krische, *Top. Organomet. Chem.* **34**, 107 (2011).
8. A. Hassan, M. J. Krische, *Org. Process Res. Dev.* **15**, 1236 (2011).
9. I. S. Kim, S. B. Han, M. J. Krische, *J. Am. Chem. Soc.* **131**, 2514 (2009).
10. X. Gao, I. A. Townsend, M. J. Krische, *J. Org. Chem.* **76**, 2350 (2011).
11. X. Gao, H. Han, M. J. Krische, *J. Am. Chem. Soc.* **133**, 12795 (2011).
12. J. R. Zbieg, T. Fukuzumi, M. J. Krische, *Adv. Synth. Catal.* **352**, 2416 (2010).
13. F. Shibahara, J. F. Bower, M. J. Krische, *J. Am. Chem. Soc.* **130**, 6338 (2008).
14. J. R. Zbieg, J. Moran, M. J. Krische, *J. Am. Chem. Soc.* **133**, 10582 (2011).
15. H. Alper, N. Hamel, *J. Am. Chem. Soc.* **112**, 2803 (1990).
16. V. Komanduri, M. J. Krische, *J. Am. Chem. Soc.* **128**, 16448 (2006).
17. G. L. Hamilton, E. J. Kang, M. Mba, F. D. Toste, *Science* **317**, 496 (2007).
18. M. Rueping, A. P. Antonchick, C. Brinkmann, *Angew. Chem. Int. Ed.* **46**, 6903 (2007).
19. S. Mukherjee, B. List, *J. Am. Chem. Soc.* **129**, 11336 (2007).
20. S. Liao, B. List, *Angew. Chem. Int. Ed.* **49**, 628 (2010).
21. G. Jiang, B. List, *Chem. Commun. (Camb.)* **47**, 10022 (2011).
22. B. Xu, S.-F. Zhu, X.-L. Xie, J.-J. Shen, Q.-L. Zhou, *Angew. Chem. Int. Ed.* **50**, 11483 (2011).
23. S. E. Denmark, J. Fu, *Chem. Rev.* **103**, 2763 (2003).
24. M. Yus, J. C. González-Gómez, F. Foubelo, *Chem. Rev.* **111**, 7774 (2011).
25. R. W. Hoffmann, W. Ladner, *Tetrahedron Lett.* **20**, 4653 (1979).
26. H. C. Brown, K. S. Bhat, *J. Am. Chem. Soc.* **108**, 293 (1986).
27. H. C. Brown, K. S. Bhat, *J. Am. Chem. Soc.* **108**, 5919 (1986).
28. H. Kim, S. Ho, J. L. Leighton, *J. Am. Chem. Soc.* **133**, 6517 (2011).
29. A. Dobson, S. R. Robinson, M. F. Uttley, *J. Chem. Soc., Dalton Trans.* **1975**, 370 (1975).
30. J. R. Zbieg, E. L. McInturff, J. C. Leung, M. J. Krische, *J. Am. Chem. Soc.* **133**, 1141 (2011).
31. H. C. Maytum, B. Tavassoli, J. M. J. Williams, *Org. Lett.* **9**, 4387 (2007).
32. K. Hiraki, N. Ochi, Y. Sasada, H. Hayashida, Y. Fuchita, S. J. Yamanaka, *Chem. Soc. Dalton Trans.* **1985**, 873 (1985).
33. P. Xue *et al*., *Organometallics* **23**, 4735 (2004).

Acknowledgments: The Robert A. Welch Foundation (grant F-0038) and the NIH's National Institute of General Medical Sciences (grant RO1-GM069445) are acknowledged for financial support.

Supplementary Materials

www.sciencemag.org/cgi/content/full/336/6079/324/DC1
Materials and Methods
Tables S1 to S4
References (*34*–*42*)

17 January 2012; accepted 8 March 2012
10.1126/science.1219274

A Universal Method to Produce Low–Work Function Electrodes for Organic Electronics

Yinhua Zhou,[1] Canek Fuentes-Hernandez,[1] Jaewon Shim,[1] Jens Meyer,[2] Anthony J. Giordano,[3] Hong Li,[3] Paul Winget,[3] Theodoros Papadopoulos,[3] Hyeunseok Cheun,[1] Jungbae Kim,[1] Mathieu Fenoll,[1,4] Amir Dindar,[1] Wojciech Haske,[1] Ehsan Najafabadi,[1] Talha M. Khan,[1] Hossein Sojoudi,[5] Stephen Barlow,[3] Samuel Graham,[5] Jean-Luc Brédas,[3] Seth R. Marder,[3] Antoine Kahn,[2] Bernard Kippelen[1]*

Organic and printed electronics technologies require conductors with a work function that is sufficiently low to facilitate the transport of electrons in and out of various optoelectronic devices. We show that surface modifiers based on polymers containing simple aliphatic amine groups substantially reduce the work function of conductors including metals, transparent conductive metal oxides, conducting polymers, and graphene. The reduction arises from physisorption of the neutral polymer, which turns the modified conductors into efficient electron-selective electrodes in organic optoelectronic devices. These polymer surface modifiers are processed in air from solution, providing an appealing alternative to chemically reactive low–work function metals. Their use can pave the way to simplified manufacturing of low-cost and large-area organic electronic technologies.

Organic-based thin-film optoelectronic devices, such as organic solar cells (OSCs), organic light-emitting diodes (OLEDs), and organic thin-film transistors (TFTs), hold great economic potential; they may lead to a new generation of consumer electronic devices that could be printed or processed at low cost on large areas, have very low weight, and conform to free-form and flexible substrates (*1*–*4*). However, most printed optoelectronic devices require at least one electrode with a work function (WF) that is sufficiently low to either inject electrons into or collect electrons from the lowest unoccupied molecular orbital (LUMO) of a given organic semiconductor. Low-WF metals, such as alkaline-earth metals (Ca, Mg) or metals co-deposited or coated with alkali elements (Li, Cs), meet this requirement; however, they are chemically very reactive and easily oxidize in the presence of ambient oxygen and

[1]Center for Organic Photonics and Electronics (COPE), School of Electrical and Computer Engineering, Georgia Institute of Technology, Atlanta, GA 30332, USA. [2]Department of Electrical Engineering, Princeton University, Princeton, NJ 08544, USA. [3]Center for Organic Photonics and Electronics (COPE), School of Chemistry and Biochemistry, Georgia Institute of Technology, Atlanta, GA 30332, USA. [4]Solvay SA, rue de Ransbeek 310, 1120 Brussels, Belgium. [5]Center for Organic Photonics and Electronics (COPE), George W. Woodruff School of Mechanical Engineering, Georgia Institute of Technology, Atlanta, GA 30332, USA.

*To whom correspondence should be addressed. E-mail: kippelen@ece.gatech.edu

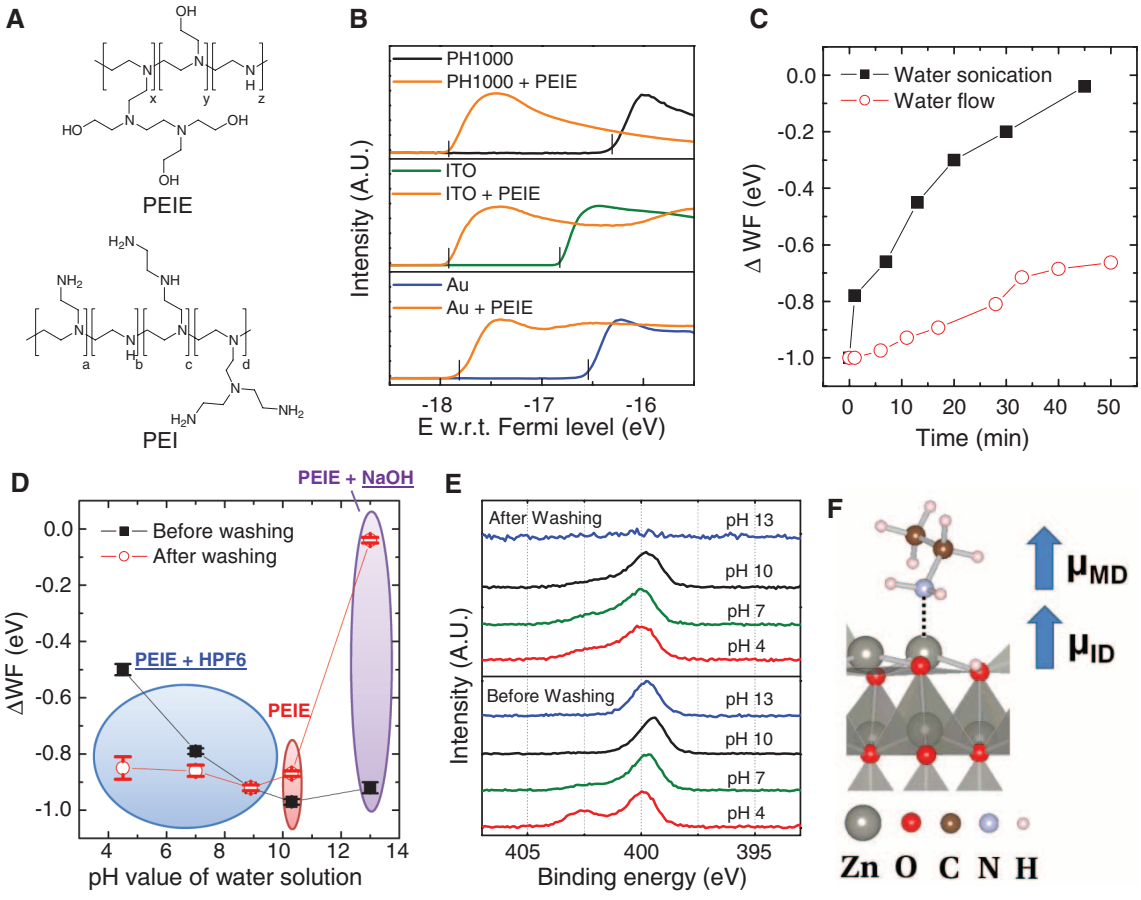

Fig. 1. (**A**) Chemical structure of PEIE and PEI. (**B**) Photoemission cutoff obtained via UPS for PEDOT:PSS PH1000, ITO, and Au samples, with and without PEIE. (**C**) WF change, relative to bare ITO, of ITO/PEIE after different washing conditions. (**D**) WF change, relative to bare ITO, upon modification from PEIE water solution, PEIE with HPF_6 water solution, and PEIE with NaOH water solution before (solid squares) and after (open circles) water washing. (**E**) N1s core level recorded via XPS on the samples in (D) before and after washing. (**F**) Proposed model of molecular dipole–induced and surface dipole–induced WF reduction on ZnO surface.

water. Thus, their use in printed electronics presents limitations that can only be overcome by the fabrication of devices in an inert atmosphere and their subsequent encapsulation with barrier-coating technologies, which increases both the cost and complexity of the device architectures.

Several strategies for replacing low-WF metals have been explored. In one approach, a film of a conducting or semiconducting material, typically thicker than 10 nm and displaying a low WF, is coated on a high-WF electrode. This film, an electron transport material, mediates charge injection and transport between the higher-WF conductive electrode onto which it is coated and a semiconducting layer in the device. Common examples of this approach have included coating indium tin oxide (ITO) with thin metal-oxide films—such as ZnO (*5*), In_2O_3 (*6*), Al-doped ZnO (*7*), or In-doped ZnO (*8*)—that present a lower WF (around 4.3 eV) than ITO. In another approach, the surface of the conductive electrode is coated with an ultrathin layer (≤10 nm) of a material that is chemically or physically adsorbed onto the conductor surface; the surface modifier is chosen in such a way as to create strong interface and/or molecular dipoles that induce a vacuum-level shift and modify the WF of the conductor. In this context, the chemisorption of small molecules onto the surface of conductors has been the most common route. For example, the WF of ITO could be decreased from 4.4 to 3.9 eV when treated with a basic solution of $N(C_4H_9)_4OH$ (*9*). The chemisorption of amine-containing conjugated small molecules such as tetrakis(dimethylamino)ethylene (TDAE) led to even greater reductions (up to 0.9 eV) of the WF of ITO (*10*), Au (*11*, *12*), and poly(3,4-ethylenedioxythiophene):poly(styrenesulfonate) (PEDOT:PSS) (*13*, *14*). However, molecules such as TDAE are highly unstable in air in their neutral state and undergo spontaneous oxidation, which limits their practical use. Chemisorbed self-assembled monolayers (SAMs) of dipolar molecules can also substantially modify the WF of metals and metal oxides (*15*–*17*), but specific surface chemistry is required to ensure chemisorption; a similar problem is faced by other inorganic-based modifiers such as Cs_2CO_3 when processed from solution (*18*). Polyethylene oxide and conjugated polymers have also been used but yield reductions in WF that are generally smaller (0.3 to 0.5 eV) (*19*–*21*).

Table 1. Work function of conducting materials with and without polymer modifiers, as independently measured by Kelvin probe in air and by UPS. Empty cells indicate no measurement for the corresponding sample.

Electrodes	Work function (eV)					
	Kelvin probe in air			UPS		
	Pristine	With PEIE	With PEI	Pristine	With PEIE	With PEI
Metal oxides						
ITO	4.62 ± 0.06	3.60 ± 0.06	3.50 ± 0.06	4.40	3.30	3.27
	5.16 ± 0.06*	3.60 ± 0.06*	—	5.00*	3.30*	—
ZnO	4.26 ± 0.06	3.28 ± 0.06	3.10 ± 0.06	3.96	3.55	3.17
FTO	4.68 ± 0.06	3.80 ± 0.06	3.60 ± 0.06	—	—	—
Metals						
Au	5.10 ± 0.10	3.90 ± 0.06	3.94 ± 0.06	4.70	3.40	—
Ag	4.60 ± 0.06	3.70 ± 0.06	3.60 ± 0.06	—	—	—
Al	3.40 ± 0.06	2.75 ± 0.06	—	—	—	—
PEDOT:PSS	4.90 ± 0.06	3.58 ± 0.06	3.88 ± 0.06	4.95	3.32	3.16
Graphene	4.60 ± 0.06	3.80 ± 0.10	—	—	—	—

*Substrate was treated with an O_2 plasma for 2 min prior to measurements or polymer modifier deposition.

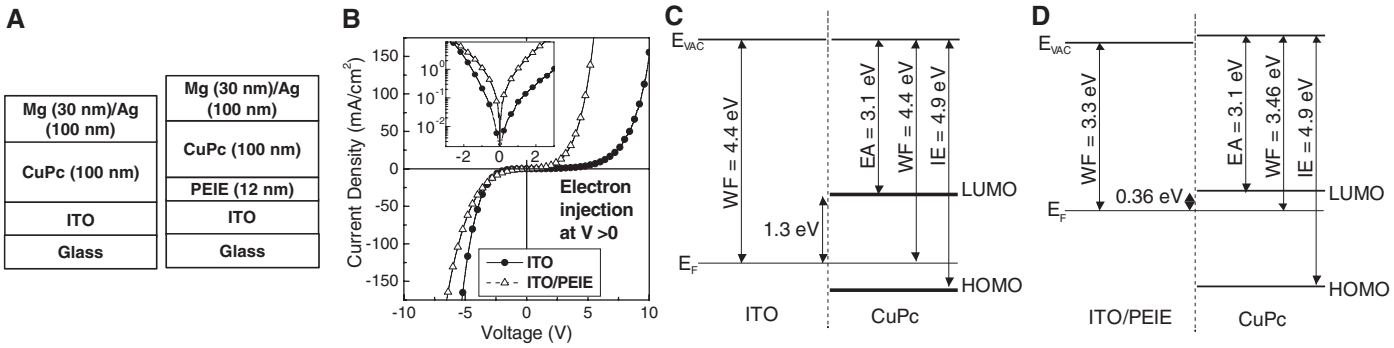

Fig. 2. (**A**) Structure of devices using ITO with and without PEIE as the bottom electrode. (**B**) *J-V* characteristics of these devices (without correction for built-in potential); inset shows the *J-V* characteristics on a semilogarithmic scale at low voltage. (**C** and **D**) Energy level alignment of CuPc (10 nm) on top of (C) ITO and (D) ITO/PEIE.

Here, we report on what appears to be a "universal" approach to reducing the WF of a conductor, in which an ultrathin layer (1 to 10 nm) of a polymer containing simple aliphatic amine groups is physisorbed onto the conductor surface. In contrast to the π-conjugated amine-containing small molecules and polymers considered earlier, the polymers exploited in this work are large band-gap insulators and should not be regarded as charge-injection layers but rather as surface modifiers. The intrinsic molecular dipole moments associated with the neutral amine groups contained in such an insulating polymer layer, and the charge-transfer character of their interaction with the conductor surface, together reduce the WF of a wide range of conductors. The commercially available polymer modifiers can be easily processed in air, from dilute solutions in environmentally friendly solvents such as water or methoxyethanol. Their low cost and ease of processing make them compatible with roll-to-roll large-area mass production techniques and suited for organic or printed electronic devices. To illustrate their potential, we evaluate their performance in various device platforms, such as OSCs (including the demonstration of all-polymeric OSCs), organic and metal-oxide TFTs, and OLEDs.

Figure 1A shows the chemical structure of polyethylenimine ethoxylated (PEIE) and branched polyethylenimine (PEI). The high content of amine groups (primary, secondary, and tertiary) in the polymer structures yields high pH values in water and methoxyethanol solutions; the pH values were measured to be 10.3 for PEIE and 10.5 for PEI in water, and 10.1 for PEIE and 10.3 for PEI in methoxyethanol solutions with a polymer concentration of 0.4 weight percent. Figure 1B displays the results of ultraviolet photoemission spectroscopy (UPS) measurements on a series of conductors before and after deposition of an ultrathin layer of PEIE; the spectra revealed WF reductions from 4.95 to 3.32 eV for PEDOT:PSS (high-conductivity grade PH1000), from 4.40 to 3.30 eV for ITO, and from 4.70 to 3.40 eV for Au. Separate Kelvin probe measurements in air further indicate that PEIE reduced the WF of metal oxides (ITO, FTO, ZnO), metals (Au, Ag, Al), and PEDOT:PSS PH1000 as well as graphene. Table 1 summarizes the values of the WF obtained by Kelvin probe and UPS experiments for several conductors modified with 10-nm-thick PEIE or PEI layers. Discrepancies between the two techniques are caused by the different atmospheres and the different experimental conditions under which the Kelvin probe and UPS experiments were conducted (*22*).

The thermal stability of the WF of PEIE- and PEI-coated ITO substrates was studied by Kelvin probe measurements in air. The WF of PEIE-coated ITO substrates did not suffer any change until a temperature of 190°C, making them compatible with the processing of printed electronic devices on plastic substrates (typically at temperatures below 200°C) (fig. S1). For PEI-coated ITO electrodes, the WF was unaffected until 150°C (fig. S1). PEIE-coated ITO electrodes also remained fairly stable under normal ambient conditions for more than 4 weeks; during that period, the WF varied by less than 0.2 eV (fig. S1). Furthermore, aqueous solutions of PEIE or PEI are stable in air (i.e., remain effective agents for reducing the WF) for more than 1 year.

Inverse photoemission spectroscopy (IPES) and UPS measurements on PEIE-coated Au indicate electron affinity and ionization potential energy values of 0.3 eV and 6.5 eV, respectively (fig. S2). These results imply that, in contrast to water/alcohol-soluble polymers based on a π-conjugated main chain that can display good electron-transporting properties (*23–26*), PEIE is likely to function as an insulator with a gap of 6.2 eV, and to exhibit large barriers for both hole and electron injection. We investigated the PEIE thickness dependence (from 2 to 22 nm) of the WF modification (ΔWF) of ITO and found a variation of <10% (fig. S3). However, even if the thickness of the PEIE layer did not influence ΔWF, its insulating nature would cause thicker polymer layers to adversely affect device performance.

Atomic force microscopy (AFM) measurements on PEIE-coated, non–plasma-treated ITO show that a 10-nm-thick PEIE layer did not uniformly cover the ITO surface, but formed islands separated by areas with a much thinner PEIE coating (fig. S4, C to F). These PEIE islands could be easily washed away by subjecting the PEIE-coated ITO substrate to a mild flow of running distilled water for 1 min (fig. S4, G and H). After washing, |ΔWF| decreased by less than 0.1 eV. This observation indicates that only an ultrathin layer of PEIE is needed to produce a large ΔWF and that the processes leading to such modifications are truly confined to the surface of the conductor.

To explore the strength of the binding between PEIE and substrate, we monitored the WF of a PEIE-coated ITO substrate over time as a function of controlled washing cycles with water. Figure 1C shows the evolution of ΔWF when the substrates were subjected to a total of 50 min of mild washing conditions (*22*). After such a period of time, |ΔWF| became less than 0.34 eV. The apparent resilience of the PEIE layer on the surface of ITO might at first glance point to a strong binding interaction between the polymer and the electrode; however, the WF reduction entirely disappeared after the PEIE-coated ITO substrate was subjected to a 50-min water wash in an ultrasonic bath (Fig. 1C). This result suggests that the PEIE layer is physisorbed on the conductor's surface, which would be consistent with the seemingly universal ability of PEIE to substantially reduce the WF of such a diverse group of conducting materials (Table 1).

To further explore the nature of the interaction between PEIE and the conductor surface, we modified the pH values of the original PEIE/water solution by adding either hexafluorophosphoric acid (HPF_6) or NaOH. PEIE was deposited on ITO from solutions with pH values of 4.5, 7.1, 9.2, 10.3, and 13. Figure 1D displays the ΔWF values induced before and after washing for 1 min with running water. Differences in the solution pH values were expected to primarily affect the degree of protonation of the amine groups in PEIE. The degree of PEIE protonation was followed with x-ray photoelectron spectroscopy (XPS) by tracking the position and shape of the N1s peak and the appearance of the F1s peak for PEIE solutions with pH values below

10.3 (fig. S5). When PEIE was processed from the most basic solution, ΔWF was −0.92 eV and the presence of neutral amine groups was indicated by the N1s peak at 399.8 eV (Fig. 1E). The same N1s peak appeared in the PEIE layers processed from a pH = 10.3 solution that yielded ΔWF = −0.97 eV. These results indicate that neutral amine groups are primarily involved in the interactions leading to the formation of the interface dipoles and the substantial changes in WF. In contrast, when the PEIE layers were processed from the more acidic solutions with a higher proportion of protonated amines, smaller WF reductions were observed. In films processed from solutions with pH values of 7.1 and 4.1, the appearance of a shoulder in the N1s peak at 402.5 eV (Fig. 1E) is indicative of protonated amines; at the same time, an F1s peak appeared, which is consistent with the inclusion of PF_6^- counterions accompanying the protonated amines (fig. S5). After a 1-min water wash, with the exception of the PEIE layer coated from the most basic solution (which was completely removed from the ITO surface), all layers yielded similar ΔWF values around −0.86 eV (Fig. 1D). The XPS spectra of these layers show N1s peaks with a similar shape and a small shoulder at 402.5 eV, as well as the disappearance of the F1s peak (fig. S5). Similar trends were found when the polymer layers were deposited on FTO (fig. S6A) or Au (fig. S6B), or with the use of HCl instead of HPF_6 (fig. S6C). Interestingly, these results are different from those in previous reports where poly(amidoamine) dendrimers reduced the WF of ITO (*27*, *28*). In those reports, it was speculated that protonated amine groups were primarily responsible for ΔWF of ITO. Our results show that in the case of PEIE, neutral amine groups are primarily responsible for the largest ΔWF observed.

To understand the possible mechanism leading to the WF decrease, we carried out density functional theory (DFT) calculations for the Au (111) surface and the polar (0002) and nonpolar (10-10) ZnO surfaces (*22*). A SAM of ethylamine ($C_2H_5NH_2$) molecules was used to model the amine-containing thin molecular layer adsorbed on the electrode surface (fig. S7). The adsorption energy per amine group is on the order of −0.47 eV for Au (111), −0.88 eV for ZnO (0002), and −0.78 eV for ZnO (10-10). In all cases, physisorption of the ethylamine groups is calculated to be energetically favored over dissociative chemisorptions (for example, by 0.7 eV on the ZnO (0002) surface), which is consistent with the experimental observations. The ΔWF values of the three model surfaces induced by a SAM of ethylamine molecules are calculated to be −1.3 eV for Au (111), −1.7 eV for ZnO (0002), and −1.7 eV for ZnO (10-10); these results are fully in line with the UPS and Kelvin probe data.

The mechanism leading to ΔWF has been analyzed by decomposing it into contributions from (i) the ethylamine molecular dipole (μ_{MD}) within the SAM along the direction perpendicular to the surface (leading to an electrostatic potential energy change denoted as ΔV_{MD}), and (ii) the dipole (μ_{ID}) formed at the interface between the molecular SAM and the electrode surface (ΔV_{ID}) (*29*–*31*) (Fig. 1F and table S1). In all instances, the contributions to ΔWF from the molecular dipole and the interface dipole were of the same order of magnitude—for instance, −0.5 eV and −0.8 eV, respectively, on Au (111). The contribution to ΔWF from the interface dipole is attributed to a slight electron transfer [0.16 e for ethylamine on Au (111), 0.07 e on ZnO (0002), and 0.06 e on ZnO (10-10)] from the amine-containing molecules to the electrode surface.

We tested PEIE-coated conductors as electrodes in various device geometries. First, we investigated the ability of PEIE-coated ITO substrates to inject electrons into an organic semiconductor. The devices comprised a 100-nm-thick layer of copper(II) phthalocyanine (CuPc, with an electron affinity of 3.1 eV) deposited on top of a glass/ITO/PEIE substrate with a top Mg/Ag electrode (WF = 3.6 eV), as shown in Fig. 2A. A comparison of the current density–voltage (*J-V*) characteristics of such devices to identical devices without the PEIE layer is shown in Fig. 2B. The voltage was applied to the top Mg/Ag contact. Devices without the PEIE layer present *J-V* characteristics resembling those of a diode because of the large energy barrier for electron injection from ITO to CuPc. Figure 2C illustrates that the energy level alignment of a CuPc (10 nm) layer deposited on top of ITO, as determined by UPS and IPES measurements, yielded a value of

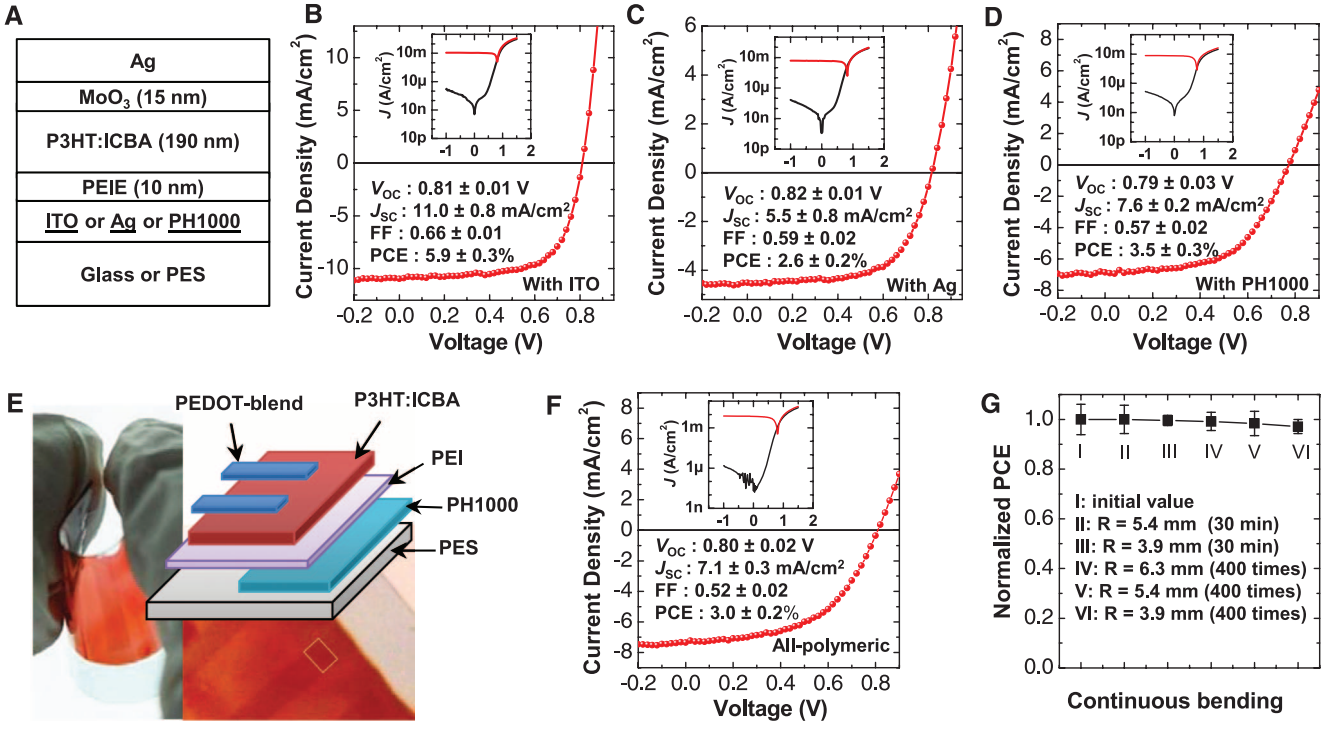

Fig. 3. (**A**) Device structure of inverted solar cells. (**B** to **D**) *J-V* characteristics of devices with PEIE-modified ITO (B), Ag (C), and PH1000 (D) electrodes under air mass (AM) 1.5 illumination (100 mW/cm^2). (**E**) Device structure and two photographs of all-polymeric solar cells. (**F**) *J-V* characteristics of all-polymeric solar cells under AM1.5 illumination (100 mW/cm^2). (**G**) Normalized PCE of all-polymeric solar cells after continuous bending tests with different bending radii (R). Insets in (B), (D), (E), and (F) are the *J-V* characteristics in the dark and under illumination on a semilogarithmic scale.

1.3 eV for the height of this barrier. In contrast, as shown in Fig. 2D, in a device with an ITO/PEIE electrode, this barrier was greatly reduced to a value of 0.36 eV. Thus, the *J-V* characteristics became nearly symmetric, with the current injected from the ITO/PEIE electrode slightly greater than that injected from Mg/Ag (Fig. 2B). This result confirms that, despite the insulating nature of PEIE, electrons can be injected efficiently into the semiconductor through the PEIE layer by processes such as tunneling or thermionic injection.

In a second step, the low-WF electrodes were tested in a variety of OSC geometries. OSCs were fabricated with PEIE-coated ITO, Ag, and PH1000 as the bottom electrode to demonstrate their electron selectivity (Fig. 3A). The top Ag layer was 150 nm for the devices with glass/ITO/PEIE and polyethersulfone (PES)/PH1000/PEIE, and it was 20 nm for the devices with glass/Ag/PEIE. A mixture of poly(3-hexylthiophene) (P3HT) and an indene-C_{60} bis-adduct (ICBA) (weight ratio 1:1) was used as the photo-active layer (*32*). Figure 3, B to D, displays the *J-V* characteristics of these solar cells in the dark and under illumination. In all cases, the *J-V* characteristics in the dark show a large rectification and small reverse saturation currents; this result demonstrates the excellent electron selectivity of the PEIE-modified electrodes. Solar cells with PEIE-coated ITO electrode (Fig. 3B) yielded a power conversion efficiency (PCE) of 5.9% [open-circuit voltage (V_{OC}) = 0.81 V, short-circuit current density (J_{SC}) = 11.0 mA/cm^2, fill factor (FF) = 0.66], averaged over 10 devices. Such a large FF value also provides indirect evidence of the good electron selectivity of the PEIE-coated ITO electrode (*33*, *34*). Note that the PCE measured in these devices is comparable with that previously reported in other inverted solar cells that use the same active layer (*35*).

We studied the shelf air stability of cells with an ITO/PEIE electrode and found that the PCE remained nearly constant after 30 days in air and was still about 70% of its initial value after 102 days (fig. S8). PEIE-coated ITO electrodes were also tested in devices with an active layer comprising a blend of poly[(4,8-bis-(2-ethylhexyloxy)-benzo[1,2-*b*:4,5-*b*′]dithiophene)-2,6-diyl-*alt*-(4-(2-ethylhexanoyl)-thieno[3,4-*b*]thiophene)-2,6-diyl] (PBDTTT-C) and 3′-phenyl-3′*H*-cyclopropa-[1,9][C_{60}-I_h][5,6]fullerene-3′-butanoic acid methyl ester ($PC_{60}BM$). Devices with an inverted architecture consisting of glass/ITO/PEIE/PBDTTT-C:$PC_{60}BM$/MoO_3/Ag yielded an average PCE of 6.6% and excellent reproducibility (fig. S9). In comparison, devices consisting of glass/ITO/PEDOT:PSS(4083)/PBDTTT-C:$PC_{60}BM$/Ca/Al yielded a PCE of 6% (fig. S9 and table S2).

In the case of the solar cells with a PEIE-coated Ag bottom electrode (Fig. 3C), light enters the device through the MoO_3 (15 nm)/Ag (20 nm) top electrode. In these devices, a relatively high FF of 0.60 was also measured but J_{SC} was lower (5.5 mA/cm^2) because of the low transmittance of the top electrode (fig. S10); as a result, the PCE was only 2.6%. Devices with a PEIE-coated PH1000 bottom electrode yielded a PCE of 3.5% (averaged over five devices), with V_{OC} = 0.79 V, FF = 0.57, and J_{SC} = 7.6 mA/cm^2. The slightly smaller FF value is attributed to the increased series resistance introduced by the relatively low conductivity of PH1000 (600 S/cm) relative to ITO or Ag, whereas the relatively small J_{SC} is mainly caused by the lower transmittance of PH1000 (*36*–*38*) and differences in the thickness of the active layer (fig. S10).

Having transformed PEDOT:PSS into an efficient electron-collecting electrode upon modification, we fabricated all-polymeric OSCs on flexible substrates [Fig. 3E and fig. S11). As shown in Fig. 3F, OSCs with PEDOT:PSS/PEI electrodes show excellent rectification in the dark in contrast to samples without PEI (fig. S12). Under illumination, semitransparent all-polymeric OSCs showed a PCE of 3.0% averaged over seven devices, with V_{OC} = 0.80 V, FF = 0.52, and J_{SC} = 7.1 mA/cm^2. When a thick Ag layer was placed behind the semitransparent OSC to reflect some of the light back into the active layer, J_{SC} increased to 8.2 mA/cm^2, yielding a PCE of 3.4% (table S3 and fig. S13), comparable to that of a device that uses a MoO_3/Ag hole-collecting electrode (Fig. 3D). Because the all-polymeric OSCs only present polymer-polymer interfaces, they demonstrate excellent mechanical properties under multiple bending conditions (Fig. 3G). They provide a proof of principle that OSCs can be fabricated using in-line, all-additive solution-based coating and/or printing of polymers. However, the design of large-area cells and modules could require the integration of some highly conductive electrodes to compensate for the lower sheet resistance of conducting polymers (*38*).

Air-stable, low-WF electrodes are also needed for organic semiconductor–based or metal oxide–based n-channel TFTs. In a TFT, the existence of large energetic barriers for electron injection at the source electrode and collection at the drain electrode can lead to a large threshold voltage (V_{TH}); it can also potentially result in low field-effect mobility (μ) when the contact resistance exceeds the channel resistance (*39*), a particularly critical issue for TFTs with short channel lengths. We fabricated examples of organic and metal-oxide n-channel TFTs that use air-stable PEIE-coated Au source and drain electrodes. In the first example, top-gate bottom-contact organic-based n-channel TFTs with a bilayer gate dielectric were fabricated (*40*) (Fig. 4A). For comparison purposes, two sets of TFTs were fabricated with Au source and drain electrodes, either coated with a PEIE layer or uncoated. In both instances, the organic semiconductor poly[*N*,*N*′-bis(2-octyldodecyl)-naphthalene-1,4:5,8-bis(dicarboximide)-2,6-diyl]-alt-5,5′-(2,2′-bithiophene) [P(NDI2OD-T2), also called N2200] (*4*) was inkjet-printed on top of the

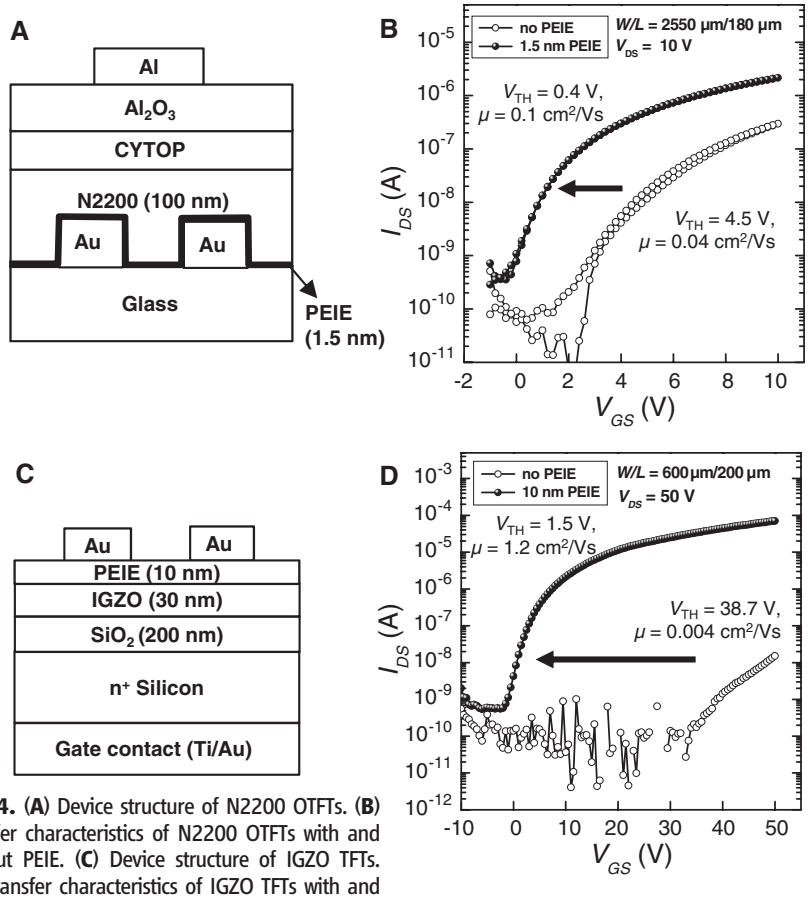

Fig. 4. (**A**) Device structure of N2200 OTFTs. (**B**) Transfer characteristics of N2200 OTFTs with and without PEIE. (**C**) Device structure of IGZO TFTs. (**D**) Transfer characteristics of IGZO TFTs with and without PEIE. CYTOP (CTL-809M) is a perfluorinated polymer purchased from Asahi Glass.

source and drain electrodes. Figure 4B displays a comparison of the transfer characteristics of both TFTs. In the TFTs with PEIE-coated source and drain electrodes, V_{TH} dropped from 4.5 to 0.4 V, the average μ increased from 0.04 to 0.1 $cm^2 V^{-1} s^{-1}$ and the device yield improved from 60% to 95%. We note that whereas μ values obtained after the PEIE modification are comparable to those of similar TFTs previously reported, the V_{TH} in our devices is lower (*4*). In this example, PEIE also coats the gate insulator inside the channel. PEIE layers thicker than 1.5 nm led to n-doping of the organic semiconductor channel. Similar doping was also observed on bottom-gate bottom-contact $PC_{60}BM$ TFTs that used PEIE-coated Au electrodes with PEIE thicknesses greater than 10 nm (fig. S14). This doping could assist the injection/collection of carriers by producing band-bending in the vicinity of the conductor surface; this effect is also likely present in OSCs containing fullerene-based acceptors (Fig. 3).

In a second example, bottom-gate top-contact amorphous InGaZnO (IGZO) TFTs were fabricated as shown in Fig. 4C. In contrast to the devices described above, PEIE was first deposited directly on top of the semiconductor (to prevent any damage from the radio frequency–sputtering deposition of IGZO) and the Au source and drain electrodes were evaporated on top of the PEIE layer. Figure 4D provides a comparison of the transfer characteristics of IGZO TFTs with and without PEIE. As in the n-channel organic-based TFTs, the V_{TH} of the IGZO TFTs dropped from 38.7 to 1.5 V and μ increased from 0.004 to 1.2 $cm^2 V^{-1} s^{-1}$ in the devices with the PEIE-modified electrodes.

Finally, we tested the use of PEIE in OLEDs by replacing a LiF/Al cathode with PEIE/Al in benchmark devices based on 4,4′-bis(carbazol-9-yl)biphenyl (CBP) and an emitter of *fac*-tris(2-phenylpyridinato-$N,C^{2'}$) iridium [$Ir(ppy)_3$], and achieved an external quantum efficiency of 15% (fig. S15). Although the performance of these devices was not optimized, it illustrates the applicability of this method to OLED platforms.

Polymers containing simple aliphatic amine groups such as PEIE and PEI appear to be "universal" surface modifiers that allow the fabrication, at very low cost and from environmentally friendly solvents, of air-stable low-WF electrodes. This approach should enable the mass production of low-WF electrodes from processes that are compatible with the large-area roll-to-roll manufacturing techniques required for the commercialization of low-cost organic and printed electronic devices. The specific properties of the polymers can be further optimized for other applications, and conceptually the approach could be applied to the development of polymers for high-WF electrodes.

References and Notes

1. H. Y. Chen *et al.*, *Nat. Photonics* **3**, 649 (2009).
2. R. H. Friend *et al.*, *Nature* **397**, 121 (1999).
3. G. Yu, J. Gao, J. C. Hummelen, F. Wudl, A. J. Heeger, *Science* **270**, 1789 (1995).
4. H. Yan *et al.*, *Nature* **457**, 679 (2009).
5. H. Cheun *et al.*, *J. Phys. Chem. C* **114**, 20713 (2010).
6. L. Wang *et al.*, *Nat. Mater.* **5**, 893 (2006).
7. J. Meyer *et al.*, *Appl. Phys. Lett.* **93**, 073308 (2008).
8. H. Cheun *et al.*, *Opt. Express* **18** (suppl. 4), A506 (2010).
9. F. Nüesch, L. J. Rothberg, E. W. Forsythe, Q. T. Le, Y. Gao, *Appl. Phys. Lett.* **74**, 880 (1999).
10. W. Osikowicz *et al.*, *Appl. Phys. Lett.* **85**, 1616 (2004).
11. L. Lindell *et al.*, *Appl. Phys. Lett.* **92**, 163302 (2008).
12. B. Bröker *et al.*, *Appl. Phys. Lett.* **93**, 243303 (2008).
13. L. Lindell *et al.*, *Chem. Mater.* **18**, 4246 (2006).
14. F. L. E. Jakobsson *et al.*, *Chem. Phys. Lett.* **433**, 110 (2006).
15. A. Sharma, P. J. Hotchkiss, S. R. Marder, B. Kippelen, *J. Appl. Phys.* **105**, 084507 (2009).
16. X. Bulliard *et al.*, *Adv. Funct. Mater.* **20**, 4381 (2010).
17. S.-N. Hsieh *et al.*, *Org. Electron.* **10**, 1626 (2009).
18. J. Huang, Z. Xu, Y. Yang, *Adv. Funct. Mater.* **17**, 1966 (2007).
19. Y. Zhou *et al.*, *Sol. Energy Mater. Sol. Cells* **93**, 497 (2009).
20. G. Jo *et al.*, *Appl. Phys. Lett.* **97**, 213301 (2010).
21. S. I. Na *et al.*, *Appl. Phys. Lett.* **97**, 223305 (2010).
22. See supplementary materials on *Science* Online.
23. F. Huang, H. B. Wu, Y. Cao, *Chem. Soc. Rev.* **39**, 2500 (2010).
24. F. Huang *et al.*, *Adv. Mater.* **19**, 2010 (2007).
25. S. H. Oh, D. Vak, S.-I. Na, T.-W. Lee, D.-Y. Kim, *Adv. Mater.* **20**, 1624 (2008).
26. W. Ma *et al.*, *Adv. Mater.* **17**, 274 (2005).
27. R. Schlapak *et al.*, *Langmuir* **23**, 8916 (2007).
28. G. Latini, M. Wykes, R. Schlapak, S. Howorka, F. Cacialli, *Appl. Phys. Lett.* **92**, 013511 (2008).
29. G. Heimel, L. Romaner, J.-L. Brédas, E. Zojer, *Phys. Rev. Lett.* **96**, 196806 (2006).
30. G. Heimel, L. Romaner, E. Zojer, J.-L. Brédas, *Acc. Chem. Res.* **41**, 721 (2008).
31. H. Li, P. Paramonov, J.-L. Brédas, *J. Mater. Chem.* **20**, 2630 (2010).
32. Y. He, H.-Y. Chen, J. Hou, Y. Li, *J. Am. Chem. Soc.* **132**, 1377 (2010).
33. H. Schmidt *et al.*, *Appl. Phys. Lett.* **96**, 243305 (2010).
34. A. Wagenpfahl, D. Rauh, M. Binder, C. Deibel, V. Dyakonov, *Phys. Rev. B* **82**, 115306 (2010).
35. Y. J. Cheng, C.-H. Hsieh, Y. He, C.-S. Hsu, Y. Li, *J. Am. Chem. Soc.* **132**, 17381 (2010).
36. Y. H. Zhou *et al.*, *Appl. Phys. Lett.* **97**, 153304 (2010).
37. O. Inganäs, *Nat. Photonics* **5**, 201 (2011).
38. S. Choi, W. J. Potscavage Jr., B. Kippelen, *Opt. Express* **18** (suppl. 3), A458 (2010).
39. A. Rolland, J. Richard, J. P. Kleider, D. Mencaraglia, *Jpn. J. Appl. Phys.* **35**, 4257 (1996).
40. D. K. Hwang *et al.*, *Adv. Mater.* **23**, 1293 (2011).

Acknowledgments: Supported by the Center for Interface Science: Solar Electric Materials, an Energy Frontier Research Center funded by the U.S. Department of Energy, Office of Science, Office of Basic Energy Sciences, under award DE-SC0001084 (Y.Z., J.S., J.M., H.C., H.L., P.W., S.B., J.-L.B., S.R.M., and S.G.), the NSF Science and Technology Centers program under agreement DMR-0120967 (C.F.-H., J.K., E.N., and A.D.), Office of Naval Research grant N00014-04-1-0120) (T.M.K. and B.K.), NSF grants DMR-1005892 (A.K.) and CMMI-0927736 (H.S.), the U.S. Department of Energy, Office of Science, Office of Basic Energy Sciences under award DE-FG02-05ER46165 (W.H. and T.P.), the Deutsche Forschungsgemeinschaft postdoctoral fellowship program (J.M.), and the National Defense Science and Engineering Graduate Fellowship program and NSF graduate research fellowship DGE-0644493 (A.J.G.).

Supplementary Materials

www.sciencemag.org/cgi/content/full/336/6079/327/DC1
Materials and Methods
Figs. S1 to S16
Tables S1 to S3
References (*41*–*52*)

6 January 2012; accepted 29 February 2012
10.1126/science.1218829

Dislocation Damping and Anisotropic Seismic Wave Attenuation in Earth's Upper Mantle

Robert J. M. Farla,[1]*† Ian Jackson,[1] John D. Fitz Gerald,[1] Ulrich H. Faul,[2] Mark E. Zimmerman[3]

Crystal defects form during tectonic deformation and are reactivated by the shear stress associated with passing seismic waves. Although these defects, known as dislocations, potentially contribute to the attenuation of seismic waves in Earth's upper mantle, evidence for dislocation damping from laboratory studies has been circumstantial. We experimentally determined the shear modulus and associated strain-energy dissipation in pre-deformed synthetic olivine aggregates under high pressures and temperatures. Enhanced high-temperature background dissipation occurred in specimens pre-deformed by dislocation creep in either compression or torsion, the enhancement being greater for prior deformation in torsion. These observations suggest the possibility of anisotropic attenuation in relatively coarse-grained rocks where olivine is or was deformed at relatively high stress by dislocation creep in Earth's upper mantle.

A rheologically weak sublithospheric mantle (the asthenosphere) is widely invoked to explain the motion of the tectonic plates on Earth [e.g., (*1*)]. Laboratory experiments underpin an emerging understanding of the anomalous seismic properties of the asthenosphere (*2*, *3*). In particular, the seismic anisotropy of this part of the upper mantle is attributed to crystallographic preferred orientation in olivine-rich rocks—testimony to their deformation by dislocation creep (*4*–*11*). Several studies have demonstrated that anelastic relaxation attributed to grain-boundary sliding can affect the shear modulus and attenuation of upper mantle rocks (*12*–*16*), but evidence for strain-energy dissipation from mechanically forced vibrations of dislocations has been largely circumstantial until now.

[1]Research School of Earth Sciences, Australian National University, Canberra, Australian Capital Territory 0200, Australia. [2]Department of Earth Sciences, Boston University, Boston, MA 002215, USA. [3]Department of Geology and Geophysics, University of Minnesota, Minneapolis, MN 55455, USA.

*To whom correspondence should be addressed. E-mail: robert.farla@yale.edu

†Present address: Department of Geology and Geophysics, Yale University, New Haven, CT 06520, USA.